J Ther Eng, Vol. 9, No. 6, pp. 1604−1617, November, 2023

Journal of Thermal Engineering
Web page info: https://jten.yildiz.edu.tr
DOI: 10.18186/thermal.1401279

Journal of Thermal Engineering

Research Article

A thermohydrodynamic performance analysis of a fluid film bearing considering with geometrical parameters

Abdurrahim DAL[1,*], Mahir ŞAHİN[1], Mustafa KILIÇ[1]

[1]*Department of Mechanical Engineering, Adana Alparslan Türkeş Science and Technology University, Adana, 01250, Türkiye*

ARTICLE INFO

Article history
Received: 10 January 2023
Revised: 15 March 2023
Accepted: 11 April 2023

Keywords:
Journal Bearing;
Thermohydrodynamic Analysis;
Bearing Geometrical Parameters

ABSTRACT

Bearing performance characteristics such as stiffness, and load capacity, are related to the lubrication fluid circulating through the gap. In the fluid film bearings, the characteristic of the lubrication film also depends on the journal geometry and the viscosity. This study aimed to research the bearing geometry influences on the thermohydrodynamic performance of a circular journal bearing. The temperature distribution is modeled using a 3-dimensional energy equation. The velocity components are obtained on the pressure distribution governed by Dowson's equation. Moreover, the heat transfer between the journal and oil is modeled with Fourier heat conduction equation, and the viscosity equation is derived for SAE10W30 commercial oil as a function of the temperature. An algorithm based on the finite difference method is developed, and a serial simulation is performed for different geometrical parameters such as bearing clearance, and bearing length-to-diameter ratio (L/D). When the radial clearance decreases from 150 μm to 100 μm, the maximum pressure grows up by 53%, and the maximum temperature decreases by 21%. On the other hand, when the L/D ratio rises from 0.8 to 1, the maximum pressure grows up by 22%, but the temperature distribution does not significantly change. The load capacity, and the stiffness are higher for low radial clearance. The load capacity, and the stiffness increase when the L/D ratio grows up.

Cite this article as: Dal A, Şahin M, Kılıç M. A thermohydrodynamic performance analysis of a fluid film bearing considering with geometrical parameters. J Ther Eng 2023;9(6):1604−1617.

INTRODUCTION

The fluid film bearing is one of the significant machine elements in modern industry, and they are generally preferred to support rotors placed in a lot of different machine from turbo-machinery to space applications. Although there have extensive area of utilization, the hydrodynamic bearings come up against some technical problems arising from high heat generation occur when they operate under high speed and heavy load conditions. Because heat generation causes a ramp down the viscosity, as well as the bearing performance, investigation of the thermal characteristics of the journal bearing-rotor system is a crucially important research area.

The load capacity and stiffness strongly depend on the lubricant viscosity directly affected by heat generation on the fluid film. Therefore, it is important that the

***Corresponding author.**
*E-mail address: adal@atu.edu.tr

This paper was recommended for publication in revised form by Regional Editor Ahmet Selim Dalkılıç

investigation of the performance of a shaft supported with hydrodynamic bearing take into account thermal effects. In the literature, there are many extensive studies on investigation of circular and non-circular hydrodynamic journal bearings considering the thermal effects [1]. Dowson et al. [2] developed an equation by considering variations of viscosity and density of lubricant. Then, Dowson et al. [2] also experimentally studied the temperature pattern of journal bearing under steady load condition. They acquired temperature data, and they measured the lubricant temperature with thermocouples at various points. Ezzat and Rohde [3] studied the three-dimensional thermohydrodynamic characteristics of a steadily loaded slider bearing. Ferron et al. [4] theoretically and experimentally analyzed thermohydrodynamic performance of a journal bearing considering with the cavitation effect and lubricant recirculation. Mitsui [5] developed an analytical method to determine the temperature distribution between the radial gap of circular journal bearings considered the cavitation effect, and investigated the rotational speed, radial gap, viscosity, and specific load influences on the lubricant film temperature. Mistry et al. [6] observed the flow of lubricant subject to the cavitation effects with an experimental study. They concluded that the modified energy equation is more successful in predicting temperature. Banwait and Chandrawat [7] theoretically analyzed a journal bearing considering the thermohydrodynamic effects. Majumdar [8] numerically investigated the thermohydrodynamic characteristics of a journal bearing. Gethin also [9] investigated the thermohydrodynamic behavior of the three-lobe journal bearing with different dissipation models under different boundary conditions, and loading directions. Li et al. [10] theoretically and experimentally investigated the thermohydrodynamic performance a turbocharger shaft supported by floating ring bearings. Chauhan et al. [11] performed a two-dimensional thermohydrodynamic analysis of elliptical bearing to compare the increase in oil-pressure, oil-temperature, and load capacity for different types of lubricant. Li et al. [12] also analyzed the misalignment effect on the static and dynamic characteristics of the bearing under thermal effects.

In the hydrodynamic bearings, the lubricant circulates through a cylindrical gap between the journal and shaft surfaces. Therefore, the geometrical properties of the cylindrical gap directly affect the flow characteristics, as expected. Moreover, these properties known as dimensional parameters of a hydrodynamic bearing such as radial clearance, bearing length to diameter ratios (L/D ratio), and inner surface properties (roughness and/or groove) determine the performance. Singh et. al. [13] theoretically investigated the thermohydrodynamic performance of a hydrodynamic journal bearing with axial groove under constant supply pressure. They investigated the effects of bearing geometry and the groove dimension on the performance with the average viscosity corresponding to the local average temperature. In addition, Sharma et. al [14] investigated thermohydrostatic performance characteristics of a hole entry hybrid journal bearing under different geometrical parameters and different operating conditions. Linjamaa et. al. [15] also modelled and analysed the effects of the elastic and the thermal deformations on the characteristics of a hybrid journal bearing. Awashi et. al. [16] studied performance of a non-recessed hybrid journal bearing for different feeding hole configurations, and they investigated the pressure distribution, flow rate, and friction characteristics of the bearing, as well as the stability of a rotor supported by the hybrid journal bearing. Brito et. al. [17] also studied the effects of the feeding condition on the performance of a hybrid bearing considering with thermal effects. Kyrkon and Nikolakopoulos [18] performed a numerical analysis for a journal bearing under different commercial oils, and they investigated the effects of the oil characteristics on the performance of the bearing. In literature, there have been many studies on investigation of performance characteristics of a hydrodynamic bearing considering with thermal effect. On the other hand, in recent days, the investigation of surface characteristics of journal-bearing is taken part in journal-bearing literature. Zhu et. al. [20] analysed thermohydrodynamic performance of a journal bearing considering surface roughness under misalignment and cavitation effects, and Mechammad et. al. [21] also researched the surface texture effects on the Thermohydrodynamic performance of the journal bearings. Although there are many studies about the investigation of geometrical parameters influences on the performance characteristics of a hybrid journal bearing [14-18], there is not comprehensive research on the investigation of the thermohydrodynamic performance characteristics of hydrodynamic bearing considering with thermal effect for different bearing geometrical parameters. However, the geometrical parameters are a crucially important role in determining the bearing performance; in addition, they also affect the thermohydrodynamic characteristics of the bearing. Therefore, it is valuable to discuss the effect of the geometrical parameters on the thermohydrodynamic characteristics considering heat transfer.

In this study, the thermohydrodynamic performance of a circular hydrodynamic bearing was numerically investigated for different geometric parameters. The lubricant flow through the radial clearance was modeled with Dowson's equation taking into account variable viscosity; the lubricant temperature field was governed by the energy equation, and the viscosity was expressed as a function of temperature. An algorithm was developed for the numerical solution of these mathematical models based on the finite difference method, simultaneously. A serial simulation was performed for different radial clearances and different L/D ratios, and the effect of the bearing parameters on the temperature and the pressure distribution, as well as load capacity and stiffness, were theoretically studied.

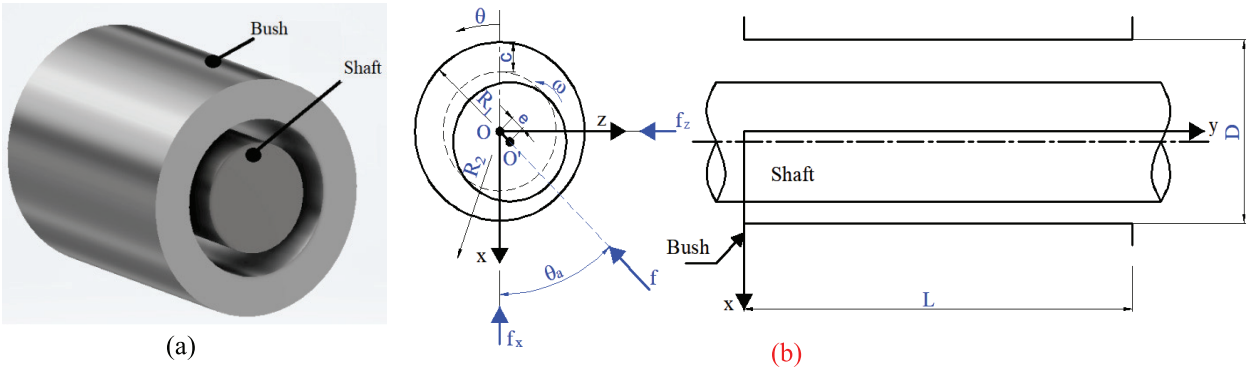

Figure 1. 3D view of journal bearing-shaft assembly, and cylindrical coordinate axes, a) isometric view, b) coordinate axis and schematic view.

MATHEMATICAL MODELS

Dowson's Equation

Figure 1 illustrates the isometric and schematic view of the shaft-bearing system and coordinate axis. Dowson's equation could be derived with continuity and Navier-Stokes equations for incompressible flow under variable viscosity, and it could be expressed with Equation 1 in the dimensionless form.

$$\frac{\partial}{\partial\theta}\left(\bar{h}^3F_2\frac{\partial\bar{p}}{\partial\theta}\right)+\frac{\partial}{\partial\xi}\left(\bar{h}^3F_2\frac{\partial\bar{p}}{\partial\xi}\right)=\Omega\frac{\partial\bar{h}}{\partial\theta}-\frac{\partial}{\partial\theta}\left(\bar{h}\frac{F_1}{F_0}\right) \quad (1)$$

where $\theta = x/R$, $\bar{\xi} = y/R$, and $\bar{z} = z/h$ are the non-dimensional cylindrical coordinates, Ω is the bearing number, and $\bar{h}$ is the non-dimensional film thickness function, and it could be written as Eq. 2.

$$\bar{h}(\theta) = 1 + \varepsilon\cos(\theta - \theta_a) \quad (2)$$

where ε is eccentricity ratio, and θ_a is attitude angle (see Figure 1). In Eq. 1, F_0, F_1, and F_2 are non-dimensional viscosity terms, and they could be expressed with following equations.

$$F_0=\int_0^1\frac{d\bar{z}}{\bar{\mu}},F_1=\int_0^1\frac{\bar{z}d\bar{z}}{\bar{\mu}},F_2=\int_0^1\frac{\bar{z}}{\bar{\mu}}\left(\bar{z}-\frac{F_1}{F_0}\right)d\bar{z}$$

where $\bar{\mu}$ is the non-dimensional viscosity.

Velocity Components

The equations of motion could be written as following expressions under the basic assumption involved that the velocity gradients $\partial u/\partial z$ and $\partial v/\partial z$ are higher than all other velocity gradients due to very thin lubrication film [13].

$$\frac{\partial p}{\partial x}=\frac{\partial}{\partial z}\left(\mu\frac{\partial u}{\partial z}\right) \quad (3)$$

$$\frac{\partial p}{\partial y}=\frac{\partial}{\partial z}\left(\mu\frac{\partial v}{\partial z}\right) \quad (4)$$

The velocity components, u and v along the coordinate axis could be obtained by integrating across the film thickness direction, z. The velocity components u and v could be derived under following boundary conditions. And they could be written as Eq. 5 and Eq. 6 in non-dimensional forms for cylindrical coordinates.

$U = 0, V = 0$ at the $z = 0$ (bush surface), and
$U = U, V = 0$ at the $z = h$ (shaft surface)

$$\bar{u}=\frac{\partial\bar{p}}{\partial\theta}\left(\int_0^{\bar{z}}\bar{h}^2\frac{\bar{z}d\bar{z}}{\bar{\mu}}-\frac{F_1}{F_0}\int_0^{\bar{z}}\bar{h}^2\frac{d\bar{z}}{\bar{\mu}}\right)+\frac{\Omega}{F_0}\int_0^{\bar{z}}\bar{h}^2\frac{d\bar{z}}{\bar{\mu}} \quad (5)$$

$$\bar{v}=\frac{\partial\bar{p}}{\partial\xi}\left(\int_0^{z}\bar{h}^2\frac{\bar{z}d\bar{z}}{\bar{\mu}}-\frac{F_1}{F_0}\int_0^{z}\bar{h}^2\frac{d\bar{z}}{\bar{\mu}}\right) \quad (6)$$

Energy Equation and Mathematical Modeling of Heat Transfer

The temperature field in the lubricant film was modelled with 3-dimensional Energy equation as similar to Ref. [4] and it could be written as Eq. 7 in non-dimensional form for cylindrical coordinate.

$$\bar{h}^2\left(\bar{u}\frac{\partial\bar{T}}{\partial\theta}+\bar{v}\frac{\partial\bar{T}}{\partial\bar{y}}+\frac{\bar{w}}{h}\frac{\partial\bar{T}}{\partial\bar{z}}-\bar{u}\frac{\bar{z}}{\bar{h}}\frac{\partial\bar{h}}{\partial\theta}\frac{\partial\bar{T}}{\partial z}\right)=$$
$$P_e\frac{\partial^2\bar{T}}{\partial\bar{z}^2}+D_e\bar{\mu}\left[\left(\frac{\partial\bar{u}}{\partial\bar{z}}\right)^2+\left(\frac{\partial\bar{v}}{\partial\bar{z}}\right)^2\right] \quad (7)$$

where $\bar{T}$ is the non-dimensional temperature, D_e is the dissipation number, and P_e is the Peclet number,.

The temperature distribution on the bush could be also modelled with 3-dimensional Fourier heat conduction equation form given as following in non-dimensional form.

$$\frac{1}{\bar{r}}\frac{\partial \bar{T}_b}{\partial \bar{r}} + \frac{\partial^2 \bar{T}_b}{\partial \bar{r}^2} + \frac{1}{\bar{r}^2}\frac{\partial^2 \bar{T}_b}{\partial \theta^2} + \frac{\partial^2 \bar{T}_b}{\partial \xi^2} = 0 \quad (8)$$

where $\bar{T}_b$ is non-dimensional bush temperature.

Viscosity Model

Viscosity of lubricant could be also computed from Eq. 9 [19], and in this study, the relation between temperature and viscosity was modelled with Eq. 10, as an empirical formula presented [16].

$$\mu_{nf} = (1 + 2.5\phi)\mu_f \quad (9)$$

$$\bar{\mu} = K_0 - K_1 T + K_2 T^2 \quad (10)$$

where K_0, K_1 and K_2 are coefficients, and they are equal to 3.287, 3.064 and 0.777, respectively.

The Load Capacity and The Stiffness

The oil film force known as the load capacity of the bearing are one of the performance parameters and it could be calculated by integrating the pressure distribution along circumferential and axial directions as given in Eq. 11 and Eq. 12.

$$\bar{f}_x = \int_0^{L/R}\int_0^{2\pi} \bar{p}(\theta,\xi)cos\theta d\theta d\xi \quad (11)$$

$$\bar{f}_y = \int_0^{L/R}\int_0^{2\pi} \bar{p}(\theta,\xi)sin\theta d\theta d\xi \quad (12)$$

where $\bar{f}_x$ and $\bar{f}_y$ are components of the dimensionless film forces along x and y directions, respectively, and the total force could be calculated as following.

$$\bar{f} = \sqrt{\bar{f}_x^2 + \bar{f}_y^2} \quad (13)$$

On the other hand, the stiffness is also an important performance characteristic, and the dimensionless stiffness could be computed form Eq. 14.

$$\bar{K} = \frac{\Delta f}{\Delta \varepsilon} \quad (14)$$

NUMERICAL SOLUTION

In order to solve the mathematical models, simultaneously, an algorithm based on the iterative numerical solution with finite difference method was developed in the presented study and the flow chart is illustrated in Figure 2. In order to accelerate the convergence of solution, the successive over relaxation method was also used in the solution of Dowson equation. The solution starts with operational conditions, initial pressure and temperature. Then, the initial viscosity and physical properties of the lubricant are calculated and the Dowson's equation is solved to obtain pressure distribution under input parameters. After the velocity components are computed on pressure distribution, the heat conduction and energy equations are solved to obtained lubricant and bush temperature. Finally, the new viscosity is calculated with the expression of the viscosity-temperature relation. This systematic solution procedure repeats until the convergence is satisfied for the viscosity.

In this study, a uniform mesh comprised of 146x24x24 nodes at the circumferential, axial, and film thickness direction, respectively, was selected for the numerical solution of mathematical models after a mesh and convergence independency study was performed for efficient solution. In numerical calculation, the following boundary conditions were defined for bearing geometry, operational and environmental conditions.

For Dowson's equation;

(1) The pressure values on edges of the journal is equal to the ambient pressure

$$\bar{p}(\theta,\xi)_{\xi=0\ and\ 1} = p_a \quad (15)$$

(2) The pressure value at the node situated in the supply hole is equal to the input pressure.

$$\bar{p}(\theta,\xi)_{supply\ hole} = \bar{p}_s \quad (16)$$

In addition, the boundary conditions on solution of energy and heat conduction equations are described as follows.

(1) On the fluid film-journal interface

$$-\frac{k_b}{R}\frac{\partial \overline{T_b}}{\partial \bar{r}}\Big|_{\bar{r}=0} = \frac{k_f}{c\bar{h}}\frac{\partial \bar{T}}{\partial \bar{z}}\Big|_{\bar{z}=0} \quad (17)$$

(2) At the fluid-shaft interface, the temperature on the fluid film is equal to shaft temperature, $\bar{T}_{\bar{z}=h} = \bar{T}_s$

(3) On the inlet hole, the temperature is equal to mixing temperature

(4) On the outer surface of the bush

$$-\frac{k_b}{R_b}\frac{\partial \bar{T}_b}{\partial \bar{r}}\Big|_{\bar{r}=R_2} = -h_b(\bar{T}_b - \bar{T}_a) \quad (18)$$

(5) At the lateral surface of the bush,

$$-\frac{k_b}{R_2}\frac{\partial T_b}{\partial \xi}\Big|_{\xi=0\ and\ 1} = -h_b(\bar{T}_b - \bar{T}_a) \quad (19)$$

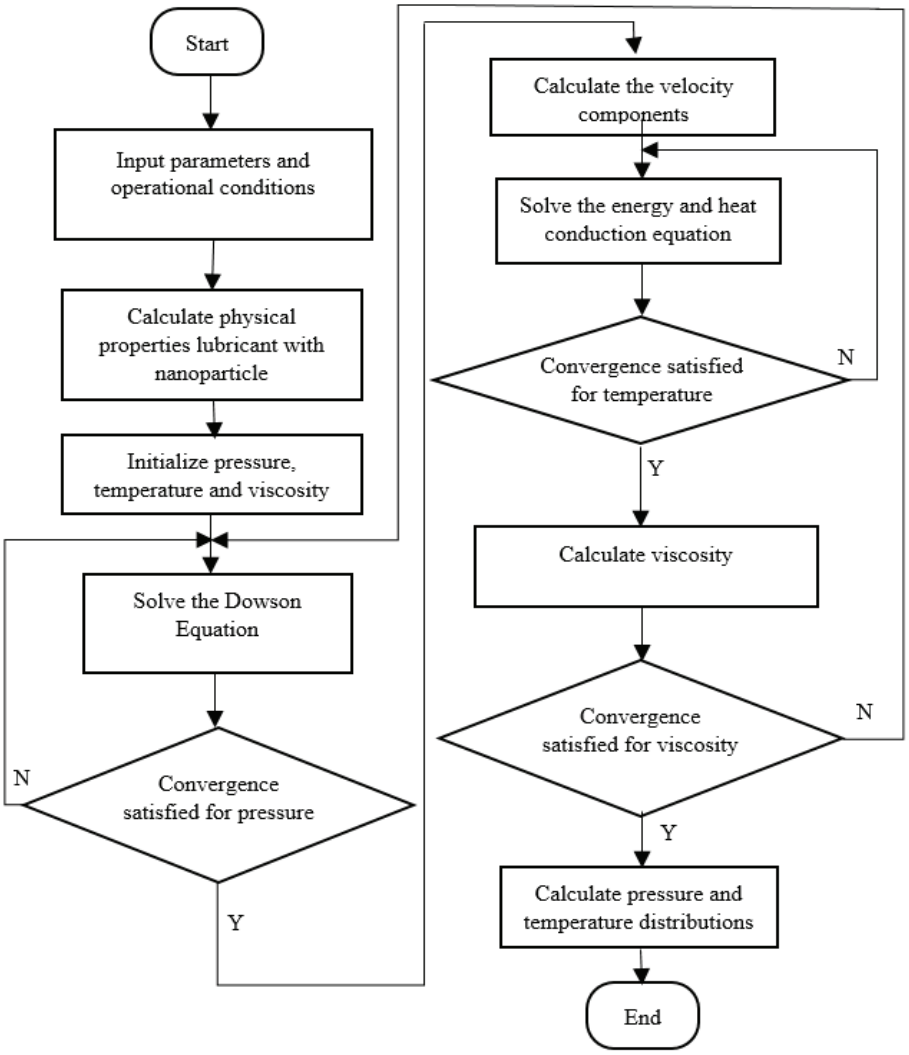

Figure 2. Flow chart of numerical solution algorithm.

In the boundary conditions, $\overline{T}_a$ and $\overline{T}_s$ are ambient and the shaft temperature, respectively, R_2 is outer radius of the bush, h_b is bush heat convection coefficient, and k_b and k_f thermal conductivity of bush and fluid film, respectively.

Validation of Numerical Calculation Procedure

A validation simulation was performed, and results were compared with measured data presented by [15], whose test parameters and conditions are listed in Table 1. The pressure and temperature variations along the circumferential axis at the middle of the bearing are shown in Figure 3a and Figure 3b. As seen in Figure 3, the simulation results are in good compliance with the measured data in both temperature and pressure variations.

RESULTS AND DISCUSSION

In this study, a thermohydrodynamic analysis was performed for a hydrodynamic journal bearing considering with influences of geometrical parameters such as bearing clearance and length/diameter ratios. A serial simulation was conducted to investigate the effect of these parameters on the temperature and the pressure distribution of the bearing-shaft system whose dimension and operational conditions are given in Table 2.

In order to investigate relation between the pressure and the temperature of the lubricant, the mathematical model was solved for pure lubricant under eccentricity ratio, ε=0.5 and rotational speed of the shaft, n=2000 rpm. The pressure distribution at the middle of the film thickness and the temperature distribution at the half of the bearing length were illustrated in Figure 4a and Figure 4b, respectively. It is seen from Figure 4a that, the pressure values increase in the region of the radial gap between the range of θ=0° and θ=150°, and they sharply decrease to the atmospheric pressure when θ exceeds 150° due to the eccentricity effect, as expected. On the other hand, the maximum pressure

Table 1. Parameters and operational conditions for the comparison study

Parameters	Value
Bearing radius, R	50 mm
Bearing length, L	80
External radius of the bearing, R_2	100 mm
Lubricant density, ρ	860 kg/m^3
Lubricant viscosity at ambient temperature, μ	0.0277 Pa.s
Thermal conductivity of the lubricant, k_f	0.13 W/m.°C
Ambient temperature, T_a	40 °C
Specific heat for lubricant, C_f	2000 J/kg.°C
Radial Clearance, c	145 μm
Thermal conductivity of the bearing, k_b	250 W/m.°C
Thermal conductivity of the shaft, k_s	50 W/m.°C
Convection of heat transfer coefficient of the bearing, h_b	80 W/m^2.°C
Thermal conductivity of the air, k_a	0.025 W/m.°C
Rotational speed, n	2000 rpm

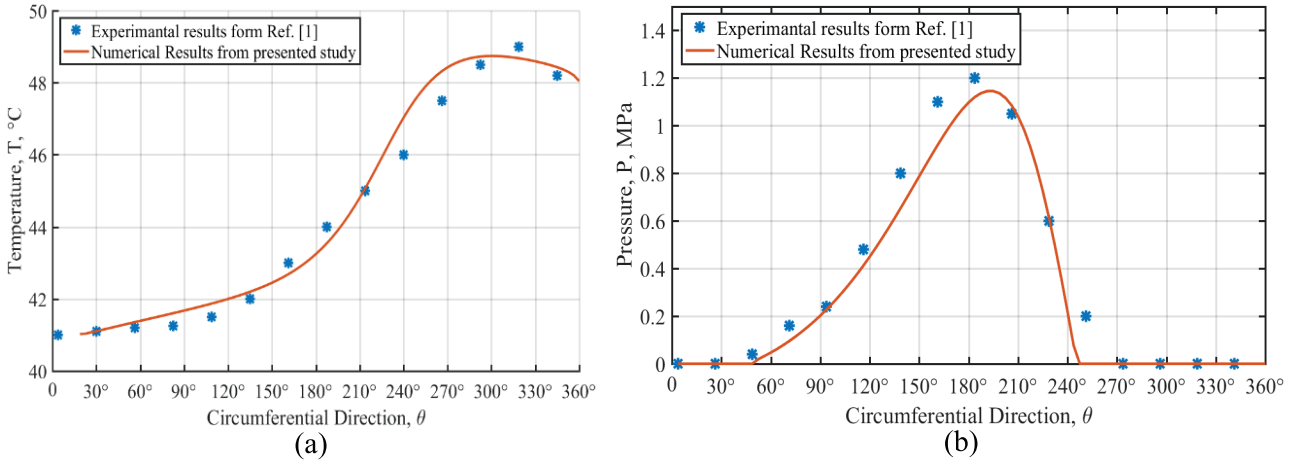

Figure 3. Temperature and pressure of variations with respect to circumferential direction at the middle of the bearing.

values occur at the left-hand side of θ=180° due to the rotational effect. On the other hand, the temperature values at the middle of the bearing with respect to circumferential direction are higher for the range of θ=180° and θ=360°, in other words maximum temperature occurs at the minimum film thickness zone, as expected (see Figure 4c and 4b). While they are equal to shaft temperature at the end of the film, z=1, they are equal to bush temperature at the z=0, as expected. In the simulation, the temperature distribution was obtained with numerical solution of the energy equation under boundary and initial conditions. Thus, the lubricant temperature is a function of fluid velocities, in other words, it depends on the pressure distribution function.

In order to research the influences of the clearance and L/D ratio on the temperature and pressure distribution, a serial simulation was performed for different radial clearance values and different L/D ratios under base lubricant, eccentricity ratio, ε=0.5. Figure 5 illustrates the temperature distribution of the bearing with an L/D ratio of 1, whereas Figure 6 illustrates the distribution of the journal bearing with an L/D ratio of 0.8 for radial clearance, c=100 μm and c=150 μm, as contour plots. It is obtained from the Figure 5a and 5b that the maximum temperature is higher for lower values of radial clearance. In addition, the higher temperature region is wider for lower value of the clearance. On the other hand, the temperature contours become wider as the L/D ratio decreases for both radial clearance values (see Figure 6). In other words, although the temperature distributions are quite similar for two different L/D ratios, it could be seen that the higher temperature regions in the

Table 2. Dimensions of the bearing-shaft system and operational conditions

Parameters	Value
Bearing radius, R	50 mm
Bearing length, L	80 mm and 100 mm
External radius of the bearing, R_2	100 mm
L/D ratio	0.8 and 1
Radial clearance, c	100 μm and 150 μm
Lubricant viscosity at ambient temperature, μ	0.0277 Pa.s
Specific heat of the oil, C_0	2000 J/kg.°C
Lubricant density, ρ	860 kg/m^3
Ambient temperature, T_a	40 °C
Thermal conductivity of the air, k_a	0.025 W/m.°C
Thermal conductivity of the lubricant, k_f	0.13 W/m.°C
Thermal conductivity of the bearing, k_b	250 W/m.°C
Thermal conductivity of the shaft, k_s	50 W/m.°C
Convection of heat transfer coefficient of the bearing, h_b	80 W/m^2.°C

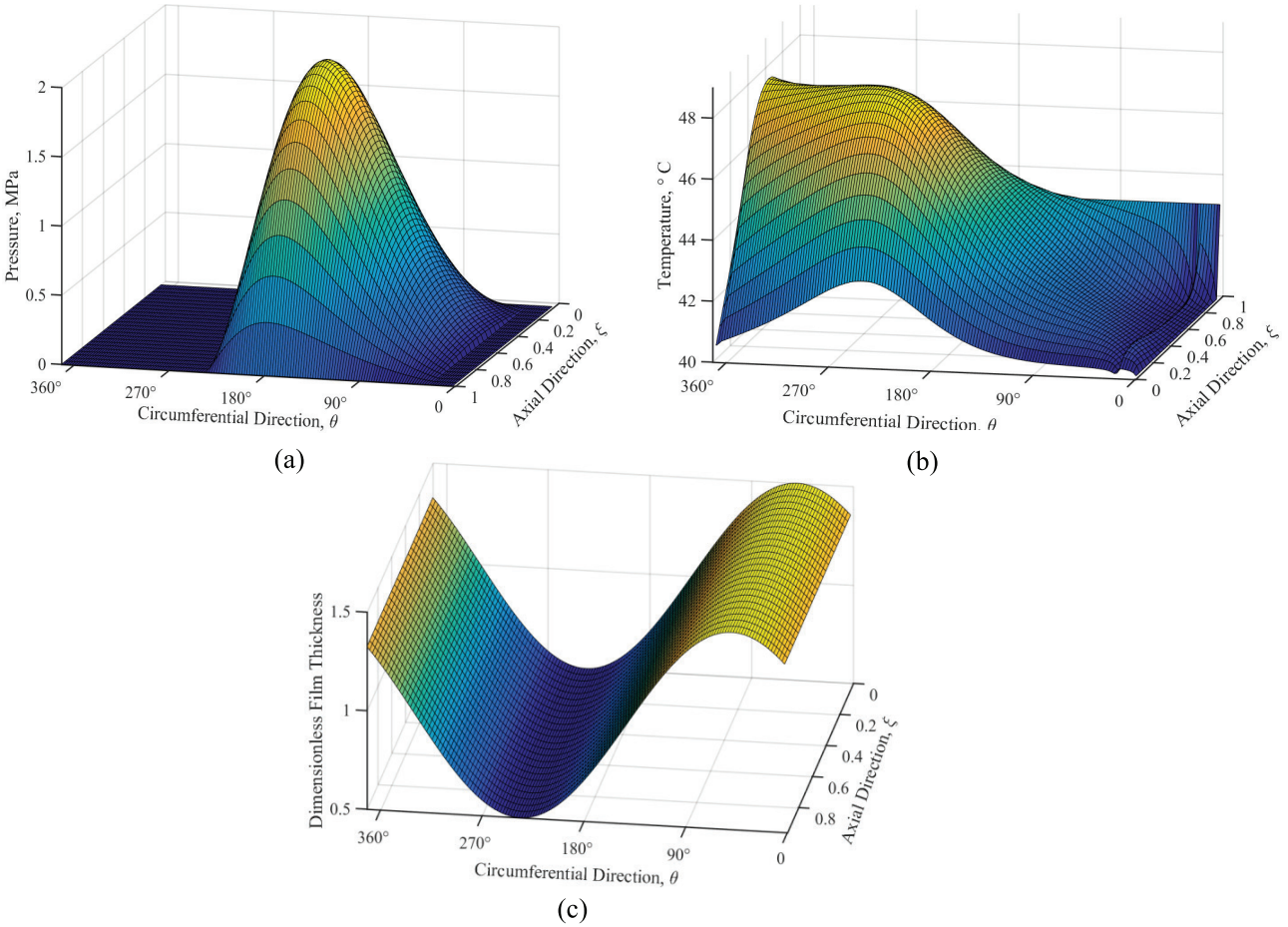

Figure 4. 3-dimensional view of a) the pressure distribution, b) the temperature distribution, c) the film thickness under ε=0.5, L/D=1, c=100 μm, n=2000 rpm.

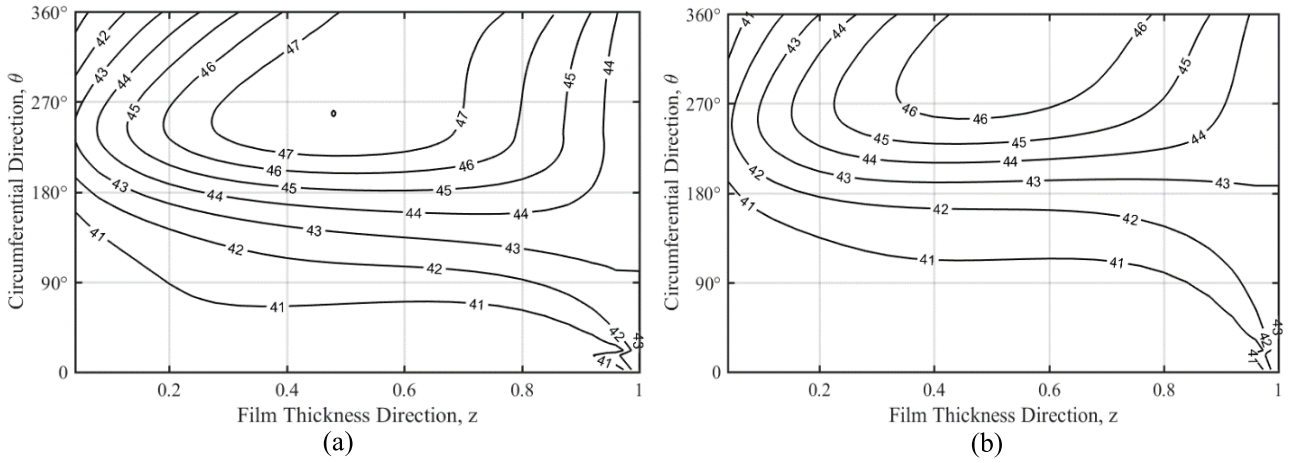

Figure 5. Temperature contours of lubricant for journal bearing L/D=1, n=2000 rpm, a) c=100 μm, b) 150 μm.

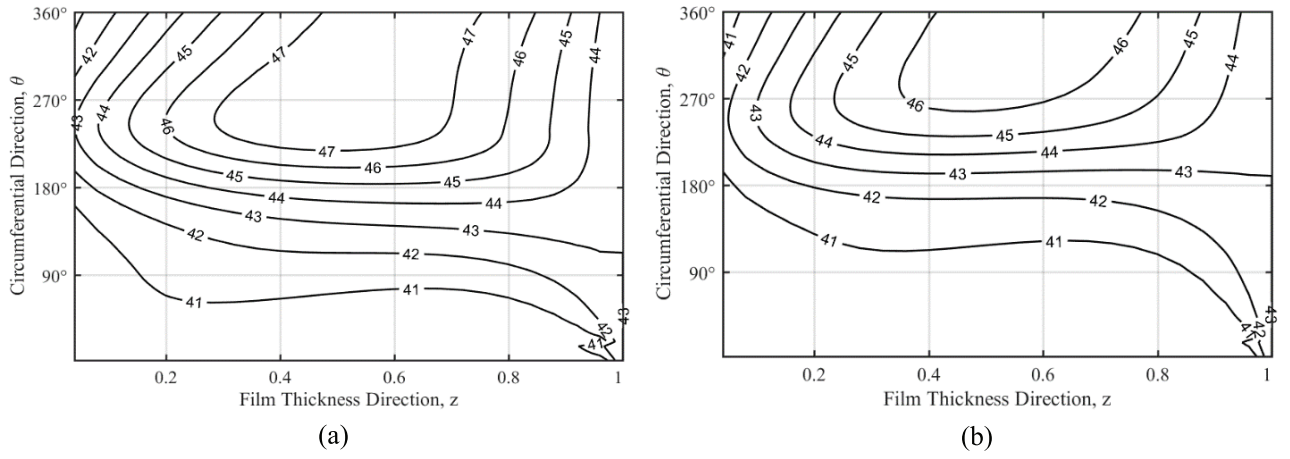

Figure 6. Temperature contours of lubricant for journal bearing L/D=0.8, n=2000 rpm, a) c=100 μm, b) 150 μm.

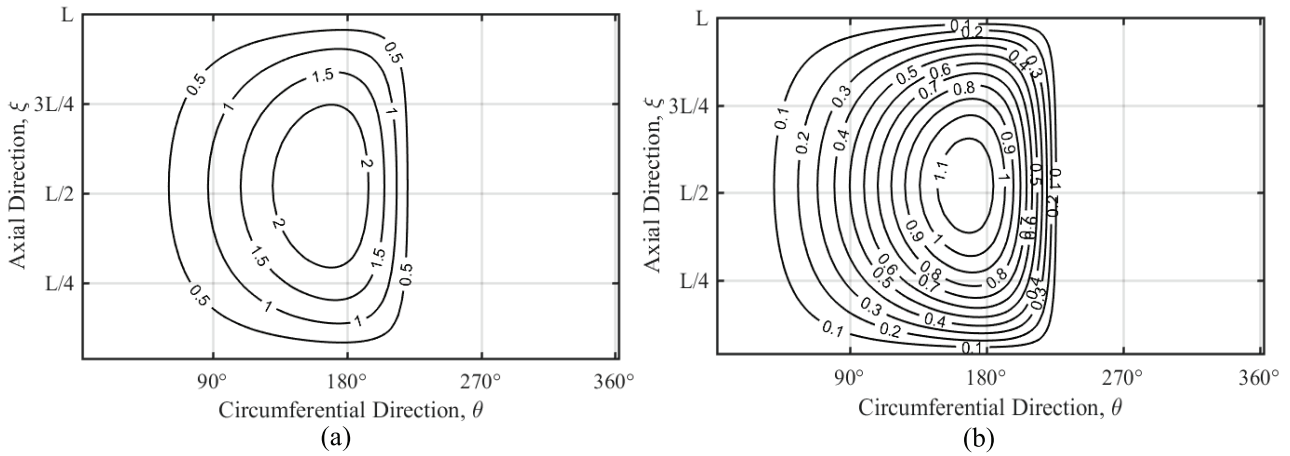

Figure 7. Pressure contours of lubricant for journal bearing L/D=1, n=2000 rpm, a) c=100 μm, b) 150 μm.

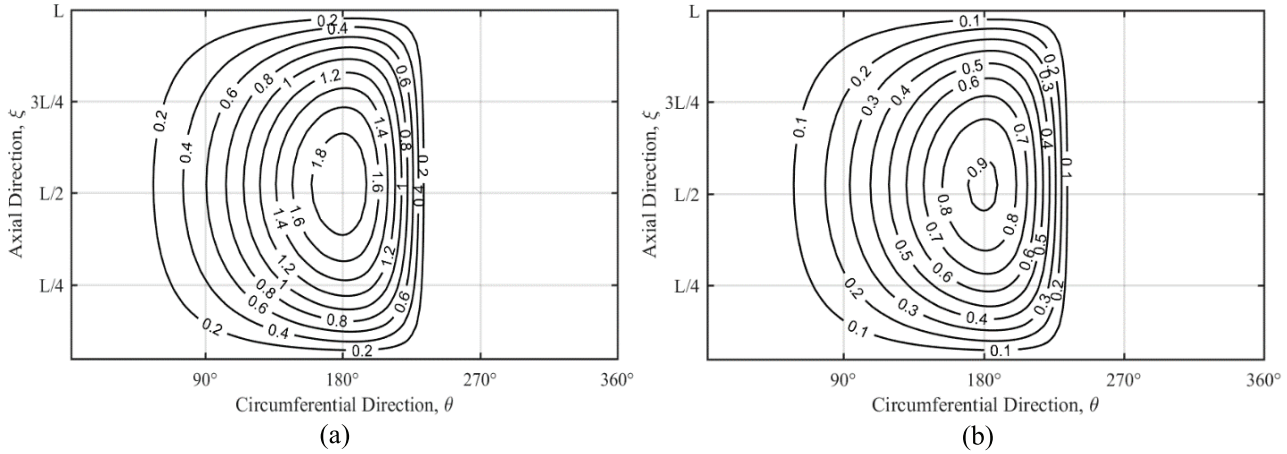

Figure 8. Pressure contours of lubricant for journal bearing L/D=0.8, n=2000 rpm, a) c=100 μm, b) 150 μm.

radial gap occur for higher values of the L/D ratio. However, it could be said that the radial clearance is more dominant in the temperature distribution than the L/D ratio. In the thermohydrodynamic lubrication analysis, the temperature distribution directly depends on the lubricant velocities, in other words, the pressure distribution. It could be seen from Figure 7 and Figure 8 that the highest-pressure values occur for lower value of radial clearance and higher value of L/D ratio. In addition, the higher-pressure region of the journal bearing with L/D of 0.8 and clearance of 100 μm is wider. Therefore, temperature values are highest for higher values of L/D ratio and lower value of the radial clearance due to the relationship between the temperature, the velocity and the pressure, as expected.

In order to investigate effects of the bearing length/diameter ratio on the pressure and the temperature distributions of the oil, a serial simulation was conducted for radial clearance, c, 100 μm under eccentricity ratio, ε, 0.35 and rotational speed, n, 2000 rpm. Figure 9a and Figure 9b show variations in the pressure and temperature values along the circumferential axis at the middle of the bearing length, respectively. As seen in Figure 9a, the L/D ratio affects the pressure distribution, but the temperature distribution does not significantly change. When the L/D ratio rises to 1, the maximum pressure grows up by 22%. Moreover, the high-pressure region in the radial gap is wider for the high value of the L/D ratio. Although the rotational speed effect on the pressure distribution is similar for both cases, in other words, the maximum pressure region shifts the left-hand side of the bearing center due to shaft rotation, the influence of the shaft speed is more dominant for the high value of L/D ratio. In addition, the temperature

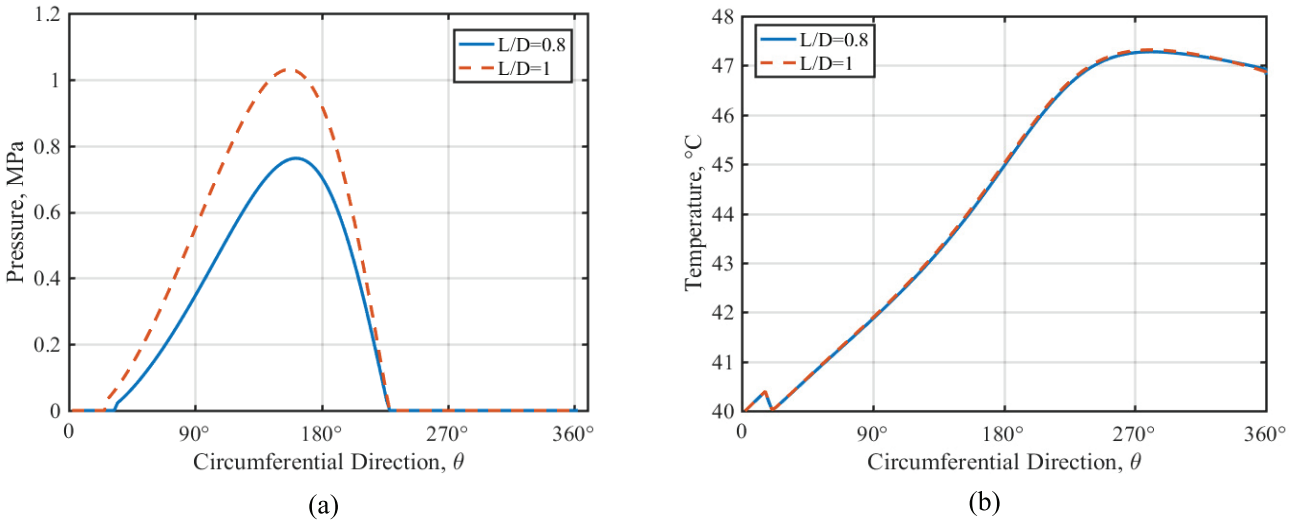

Figure 9. The pressure and temperature variations along the circumferential axis for different L/D ratios under c=100 μm, ε=0.35, and n=2000 rpm.

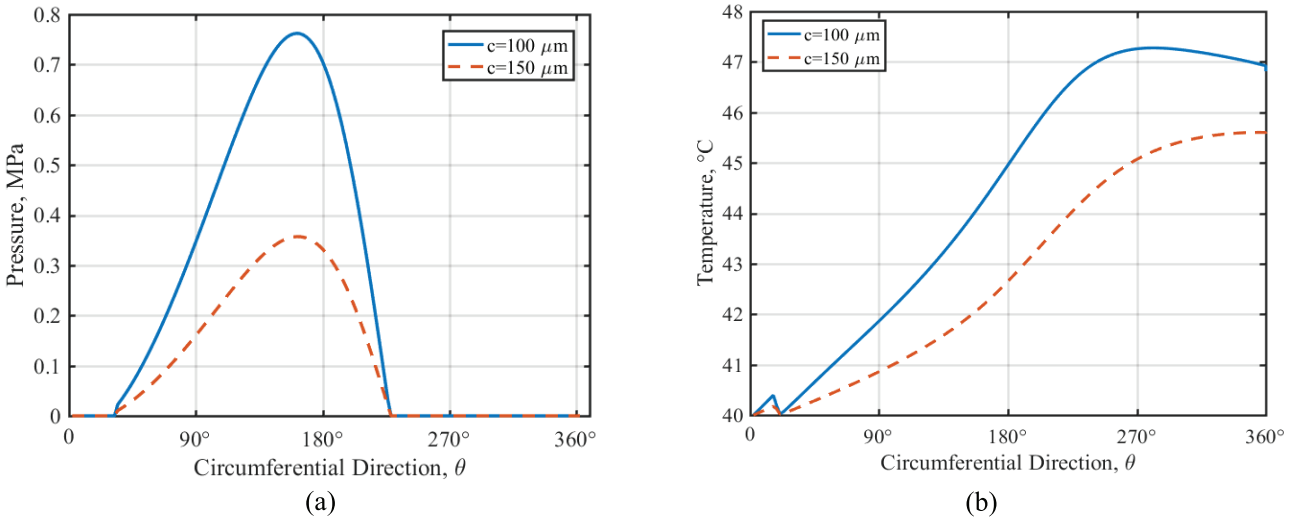

Figure 10. The pressure and temperature variations along the circumferential axis for different radial clearance values under ε=0.35, n=2000 rpm, and L/D=0.8.

variations along circumferential direction are quite similar for both L/D ratios. On the other hand, the temperature of the lubricant in the radial gap rises up when the film thickness becomes shrink, and the maximum temperature exists at the minimum film thickness for both cases. For narrow film thicknesses, the surfaces are closer, the hydrodynamic boundary layer is also smaller, and thus the heat transfer increases between surfaces.

Figure 10a and Figure 10b show variations in the pressure and temperature values along the circumferential axis at the middle of the bearing length for different radial clearances under L/D ratio, 0.8, eccentricity ratio, ε, 0.35, and rotational speed, n, 2000 rpm, respectively. As seen in Figure 10a and Figure 10b, the radial clearance affects the pressure distribution, as well as the temperature distribution. When the radial clearance decreases from 150 μm to 100 μm, the maximum pressure grows up by 53%. Therefore, the high-pressure region in the radial gap is wider for the lower value of radial clearance. In addition, rotational speed effects on the pressure distribution are also seen in Figure 10a. The radial clearance of the journal bearing is a critical geometrical parameter that affects the pressure distribution, as well as the performance. The oil circulated in the radial gap will be more squeezed when the gap is narrow, as expected. On the other hand, as similar to characteristic of the pressure distribution, the temperature variations are higher for lower value of radial clearance (see Figure 10b). When the radial clearance equals 150 μm the maximum temperature decreases by 21%. The shaft and journal surfaces are closer for low radial clearance. Therefore, the hydrodynamic boundary layer is also small, and the temperature of oil in the gap is higher. Moreover, when the film thickness becomes shrinks temperature values along the circumferential direction increase because the hydrodynamic boundary layer gets smaller for both cases. However, the temperature rising is sharper for low radial clearance.

Figure 11 shows the maximum pressure and the maximum temperature variations with respect to the eccentricity for different L/D ratios. The maximum temperature and the maximum pressure values nonlinearly increase when eccentricity ratio grows up for both cases. Besides, variations of the maximum pressure and temperature values of the bearing with an L/D ratio of 1 are higher than variations of the bearing with an L/D ratio of 0.8. As seen in Figure 11a and 11b, the difference between curves of the maximum pressure variation rises up when the eccentricity increases. On the other hand, the maximum temperature values are almost the same for low eccentricity, but the difference between curves of the maximum temperature variations grows up when eccentricity increases. Therefore, the effect of the L/D ratio on the maximum pressure is more dominant than its effect on the maximum temperature.

Figure 12a and Figure 12b show the maximum pressure and the maximum temperature variations of with respect to the eccentricity for different radial clearance values. The maximum pressure values and the maximum temperature values increase for both cases when the eccentricity rises up. On the other hand, the maximum temperature and pressure values for the journal bearing whose radial clearance is 100 μm are greater than the values of the journal bearing whose radial clearance is 150 μm. Moreover, the increase of the maximum pressure values is sharper for low radial clearance. In other words, the difference between curves of the maximum pressure variations increases when the eccentricity grows up. However, the distinction between maximum temperature curves closes, when the eccentricity ratio grows up.

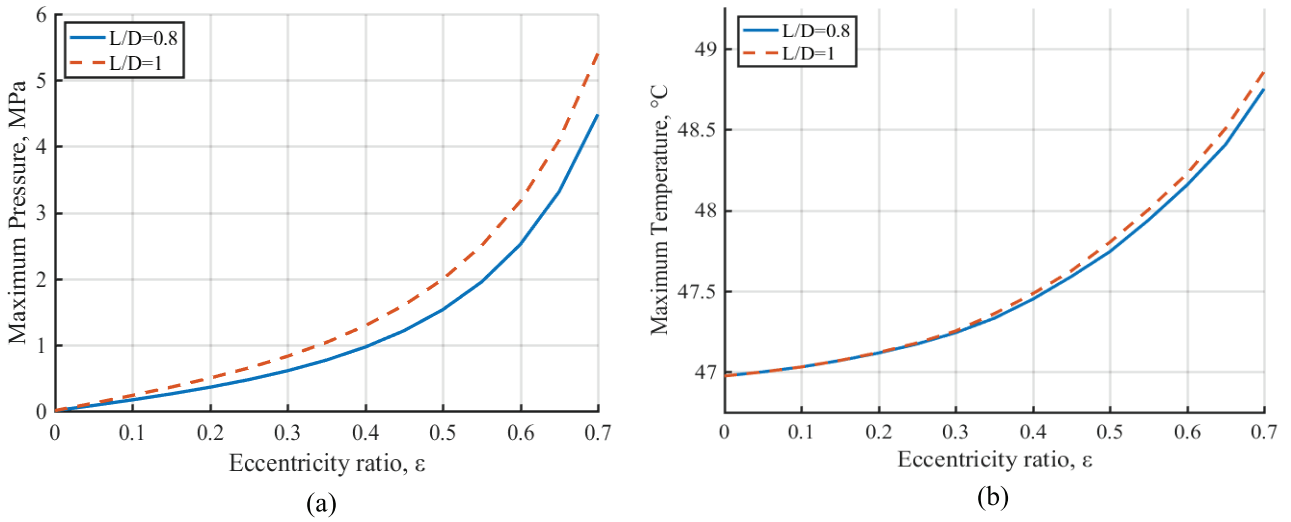

Figure 11. Maximum temperature and maximum pressure variations with respect to eccentricity for different L/D ratios, under n=2000 rpm and c=100 μm.

In the bearings, the radial gap between the surfaces directly determines the flow characteristics. In addition, because the shaft positions in the journal affect the radial gap, the eccentricity is another important parameter that affected the flow characteristics. When the eccentricity ratio grows up, the distance between the surfaces decreases, and so the pressure values increase. Because the radial gap across the eccentricity direction becomes shrinks, the lubricant squeezes more at this region (see Figure 4c). On the other hand, the temperature of the lubricant that flows through the radial gap depends on thermal properties of the lubricant, film thickness and fluid velocity in other words, the pressure distribution. On the other hand, the journal and shaft surfaces get closer and the thickness of the lubricant film becomes shrinks, as the eccentricity ratio grows up. In addition, hydrodynamic boundary layer also gets smaller. Therefore, thermal boundary layer thickness increases with increasing eccentricity ratio.

In order to analyze the effect of the geometrical parameters on the performance characteristics of the bearing, the load capacity and the stiffness were computed from Eq. 13 and Eq. 14, respectively. Figure 13 shows the load capacity and the stiffness variations with respect to eccentricity for different L/D ratios and different radial clearance values.

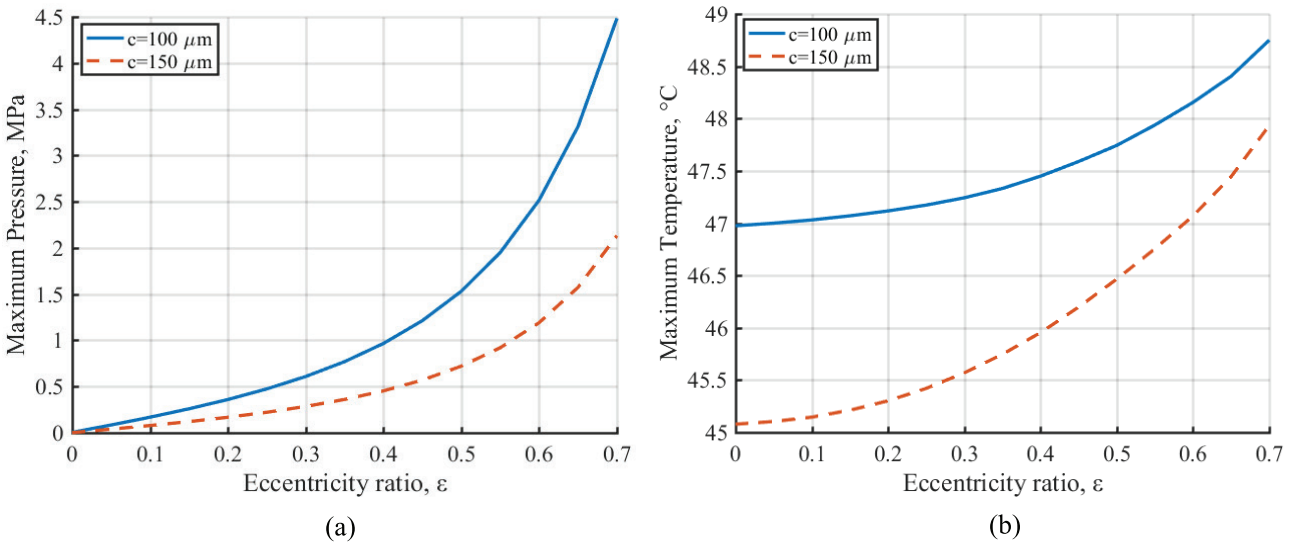

Figure 12. Maximum temperature and maximum pressure variations with respect to eccentricity for different radial clearance values under n=2000 rpm and L/D=0.8.

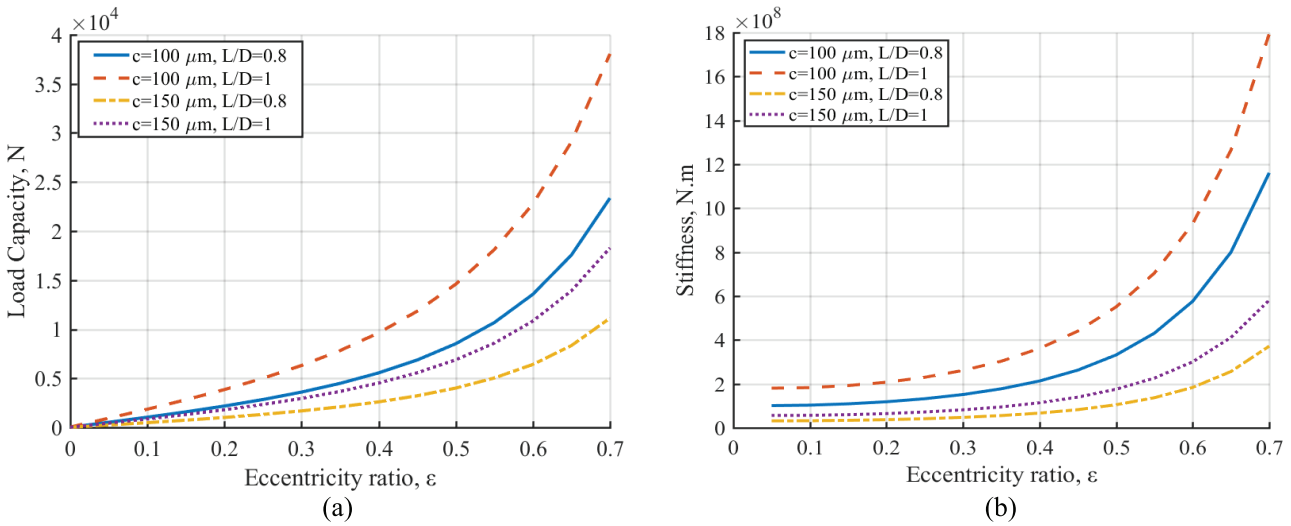

Figure 13. Load capacity and stiffness variations with respect to eccentricity ratio for different geometrical parameters.

The load capacity and the stiffness nonlinearly increase for all cases when the eccentricity grows up, as expected. On the other hand, the bearing whose radial clearance is 100 μm and L/D ratio is one has the highest load capacity and the stiffness. In other words, the decrease of radial clearance value and increase of the L/D ratio is raised the load capacity, as well as the stiffness. Besides, even if the L/D decreases from 1 to 0.8, the load and the stiffness are higher for small radial clearance. Because the load capacity and the stiffness are directly functions of the pressure distribution, the effects of the geometrical parameter on the performance characteristics are mimetic to the influences on the pressure distribution.

CONCLUSION

At this study, a thermohydrodynamic performance analysis of a journal bearing was numerically performed for different geometrical parameters. The lubricant flow was modeled with Dowson's equation, the lubricant temperature field was governed by the 3D-energy equation, and the heat transfer between the journal surface and lubricant was taken into account with the mathematical model derived with the Fourier heat conduction equation. An algorithm was also developed for the numerical solution of these mathematical models based on the finite difference method, simultaneously. To researched effects of geometrical parameters on the thermohydrodynamic characteristics of the bearing, a serial simulation was performed, and the following consequences could be deduced from the numerical results;

(1) Although the pressure values in the radial gap increase for a high L/D ratio, the temperature values are not significantly affected. However, the pressure and the temperature rise up when the radial clearance decreases. Moreover, the effect of the radial clearance on the pressure and the temperature distribution is more dominant.

(2) The maximum temperature and the pressure values nonlinearly grow when the eccentricity ratio increases. Although the radial clearance strongly influences the variations of the maximum pressure and temperature, the effect of the L/D ratio on variations is weak.

(3) When the radial clearance decreases, the difference between the maximum pressure variations with respect to eccentricity rises up, whereas the difference between the maximum temperature variations decreases.

(4) The load capacity and stiffness are increased with a high L/D ratio and low radial clearance. Moreover, the load capacity and the stiffness grow up, when the eccentricity increases.

NOMENCLATURE

c	Radial clearance, m
C	Specific heat, kJ / kg °C
D	Inner diameter of bush, m
De	Dissipation number, $P_s/(\rho_{nf} C_{nf} T_a)$
e	Eccentricity
h	Film thickness function
h_b	Convection of heat transfer coefficient of the bush, W / m² °C
$\overline{h}$	Non-dimensional film thickness function, h/c
k_b	Thermal conductivity of bush, W / m °C
k_f	Thermal conductivity of fluid, W / m °C
L	Bearing length, m
n	Rotating speed, rpm
P	Lubricant pressure, MPa
$\overline{P}$	Non-dimensional pressure, P/Ps
P_s	Oil supply pressure, MPa
Pe	Peclet number, $k_f R^2 \mu_{nf}/(C_{nf} \rho_{nf} P_s c^4)$

$\bar{T}$

$\bar{r}$	Non-dimensional cylindrical coordinate axis, r/R
R	Inner radius of bush, m
R_2	Outer radius of bush, m
T	Temperature, °C
$\bar{T}$	Non-dimensional temperature, T/T_a
u, v, w	Lubricant velocities along the x-, y-, and z-direction, respectively, m/s
x, y, z	Cartesian coordinate axis
$\bar{z}$	Non-dimensional coordinate axis, z/h

Greek symbols

ϵ	Eccentricity ratio, e/c
μ	Viscosity, $Pa.s$
$\bar{\mu}$	Non-dimensional viscosity, μ/μ_f
θ	Non-dimensional circumferential axis, x/R
θ_a	Attitude angle, rad
ω	Rotational speed, rad/s
ρ	Density, kg/m^3
ξ	Non-dimensional axial axis, y/R
Ω	Bearing number, $(\omega\mu_{nf}/P_s)\ (R/c)^2$

Subscripts

a	Refers to ambient
b	Refers to bush
f	Refers to lubricant fluid
s	Refers to shaft
$\bar{f}$	Refers to load capacity
$\bar{K}$	Refers to stiffness

AUTHORSHIP CONTRIBUTIONS

Authors equally contributed to this work.

DATA AVAILABILITY STATEMENT

The authors confirm that the data that supports the findings of this study are available within the article. Raw data that support the finding of this study are available from the corresponding author, upon reasonable request.

CONFLICT OF INTEREST

The author declared no potential conflicts of interest with respect to the research, authorship, and/or publication of this article.

ETHICS

There are no ethical issues with the publication of this manuscript.

REFERENCES

[1] Dang RK, Goyal D, Chauhan A, Dhami SS. Numerical and experimental studies on performance enhancement of journal bearings using nanoparticles based lubricants. Arch Comput Methods Eng 2021;28:3887−3915. [CrossRef]

[2] Dowson D, Hudson JD, Hunter B, March CN. An experimental investigation of the thermal equilibrium of steadily loaded journal bearings. Proc Inst Mech Eng Conf Proc 1966;181:70−80. [CrossRef]

[3] Ezzat HA, Rohde SM. A study of the thermohydrodynamic performance of finite slider bearings. ASME J Lubr Tech 1973;95:298−307. [CrossRef]

[4] Ferron J, Frene J, Boncompain R. A study of the thermohydrodynamic performance of a plain journal bearing: comparison between theory and experiments. ASME J Lubr Tech 1983;105:422−428. [CrossRef]

[5] Mitsui JI. A study of thermohydrodynamic lubrication in a circular journal bearing. Tribol Int 1987;20:331-341. [CrossRef]

[6] Mistry K, Biswas S, Athre K. Study of thermal profile and cavitation in a circular journal bearing. Wear 1992;159:79−87. [CrossRef]

[7] Banwait SS, Chandrawat HN. Study of thermal boundary conditions for a plain journal bearing. Tribol Int 1998;31:289−296. [CrossRef]

[8] Majumdar BC. The thermohydrodynamic solution of oil journal bearings. Wear 1975;31:287−294. [CrossRef]

[9] Gethin DT. Modelling the thermohydrodynamic behavior of high-speed journal bearings. Tribol Int 1996;29:579−596. [CrossRef]

[10] Li, Y, Liang F, Zhou Y, Ding S, Du F, Zhou M, et al. Numerical and experimental investigation on thermohydrodynamic performance of turbocharger rotor-bearing system. Appl Therm Eng 2017;121:27−38. [CrossRef]

[11] Chauhan A, Sehgal R, Sharma RK. Thermohydrodynamic analysis of elliptical journal bearing with different grade oils. Tribol Int 2010;43:1970−1977. [CrossRef]

[12] Li B, Sun J, Zhu S, Fu Y, Zhao X, Wang H, et al. Thermohydrodynamic lubrication analysis of misaligned journal bearing considering the axial movement of the journal. Tribol Int 2019;135:397−407. [CrossRef]

[13] Singh U, Roy L, Sahu M. Steady-state thermo-hydrodynamic analysis of cylindrical fluid film journal bearing with an axial groove. Tribol Int 2008;41:1135−1144. [CrossRef]

[14] Sharma SC, Kumar V, Jain SC, Nagaraju T. Study of hole-entry hybrid journal bearing system considering combined influence of thermal and elastic effects. Tribol Int 2003;36:903−920. [CrossRef]

[15] Linjamaa A, Lehtovaara A, Larsson R, Kallio M, Söchting S. Modelling and analysis of elastic and thermal deformations of a hybrid journal bearing. Tribol Int 2018;118:451−457. [CrossRef]

[16] Awasthi RK, Sharma SC, Jain SC. Performance of worn non-recessed hole-entry hybrid journal bearings. Tribol Int 2007;40:717−734. [CrossRef]

[17] Brito FP, Miranda AS, Claro JCP. The role of lubricant feeding conditions on the performance improvement and friction reduction of journal bearings. Tribol Int 2014;72:65−82. [CrossRef]
[18] Kyrkou ME, Nikolakopoulos PG. Simulation of thermo-hydrodynamic behavior of journal bearings, lubricating with commercial oils of different performance. Simul Model Pract Theory 2020;104:102128. [CrossRef]
[19] Einstein A. Eine neue bestimmung der Molekuldimensionen. Ann Phys 1906;324:289-306. [CrossRef]
[20] Zhu S, Zhang X. Thermohydrodynamic lubrication analysis of misaligned journal bearing considering surface roughness and couple stress. Proc Inst Mech Eng J 2022;236:2243−2260. [CrossRef]
[21] Muchammad M, Tauviqirrahman M, Mario L, Jamari J. Thermo-hydrodynamic analysis of multistep texture effect on the performance of journal bearings through acoustic and tribological characteristics. J Braz Soc Mech Sci Eng 2022;44:310. [CrossRef]